Macromolecules

pubs.acs.org/Macromolecules Article

Impact of Ionic Modifications on Polyimide Properties for Gas Separation Applications

Sudhir Ravula, Fidel E. Rodríguez-González, Pravin S. Shinde, Ana L. Montero-Alejo, Claudio A. Terraza, Sree Laxmi, Sergey Vasenkov, Kathryn E. O'Harra, Alain Tundidor-Camba,* and Jason E. Bara*

Cite This: *Macromolecules* 2024, 57, 11085−11096 Read Online

ACCESS | Metrics & More | Article Recommendations | Supporting Information

ABSTRACT: In this study, we report the synthesis and investigate the structural and gas transport characteristics of polyimides containing an imidazole ring in the main chain. First, a neutral polyimide (**PI-Im-6FDA**) was synthesized through polycondensation, followed by quaternation of the imidazole rings, producing an ionic-polyimide (**PI-Im(Me)-6FDA**). Interestingly, although the neutral form of the polyimide was able to form free-standing films, the ionic-polyimide was not able to form a self-standing film by itself. However, when free ionic liquid (IL) was added, good quality self-standing films were readily achieved (**PI-Im(Me)-6FDA** + IL). These three materials exhibited significant thermal stability, with a 10% weight loss occurring only when $T > 400$ °C. The solubility profiles of the polymers in various solvents demonstrated that the ionic modification enhances solubility in common organic solvents like acetone. The molecular weights were determined to be 91 kDa for **PI-Im-6FDA** and 84 kDa for **PI-Im(Me)-6FDA**, indicating substantial polymeric chain lengths. Additionally, computational simulations indicate an increase in density and a decrease in free volume fraction with ionic content, suggesting a more compact polymer structure, as evidenced by reduced *d*-spacing values. Further, macroscopic gas transport measurements show that **PI-Im-6FDA** exhibited superior overall permselectivity performance, while **PI-Im(Me)-6FDA** + **IL** enhances the permeability of larger gases like CH_4 and N_2, making it a promising material for specific gas separation applications. Microscopic self-diffusion measurements performed by pulsed field gradient nuclear magnetic resonance (PFG NMR) techniques reveal a significant increase in the gas self-diffusivity upon IL addition. This result is in qualitative agreement with the transport diffusivity data from the macroscopic transport measurements. PFG NMR data also show that all materials have uniform transport properties on the length scales exceeding the smallest values of the root mean square displacements (1−2 μm) used in the measurements.

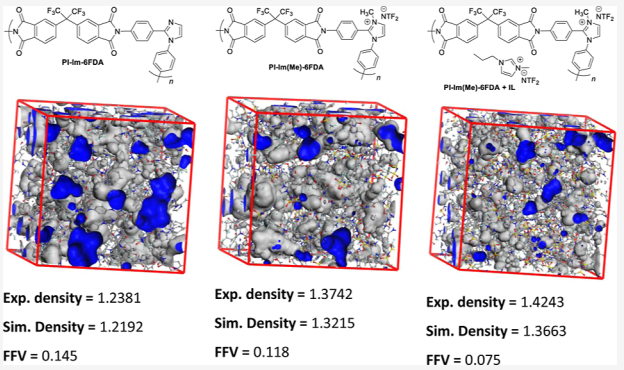

INTRODUCTION

Over a period of years, a range of materials, including polymers, metals, ceramics, and hybrids, have been employed in the production of membranes. Notably, polymers are the most commonly used materials in large-scale membrane applications.[1] Toward this, numerous polymers have been explored as materials for gas separation membranes, yet only a select few have achieved commercial viability. Among these successful materials are rubbery polymers like poly(dimethylsiloxane) and glassy polymers such as polysulfone, poly(phenylene oxide) (PPO), cellulose acetate (CA), and polyimides (PIs).[2]

PIs are a class of high-performance polymers characterized by exceptional thermal stability, mechanical properties, and chemical resistance.[3,4] The versatility of PI polymers lies in their tunability of properties through various functionalized monomers (dianhydrides and diamines) to suit specific applications. For instance, employing 4,4′-(hexafluoroisopropylidene)diphthalic anhydride (6FDA) as a monomer resulted in a high gas separation capacity due to the $-CF_3$ groups. The functional groups inhibit the torsional movement of adjacent phenyl rings, thereby hindering the effective packing of the chains. This results in a high fractional free volume (FFV) within the polymeric matrix, which subsequently enhances gas permeabilities.[5−8] On the other hand, utilizing diamine monomers containing hindered groups at the ortho position to the $-NH_2$ reduces the free rotation at the imide linkage in the PI, enabling high permeability (P) values.[9−11]

Polymeric ionic liquids (Poly(IL)s) are a novel class of polyelectrolytes synthesized via the polymerization of IL

Received: September 23, 2024
Revised: November 13, 2024
Accepted: November 20, 2024
Published: November 28, 2024

https://doi.org/10.1021/acs.macromol.4c02315
Macromolecules 2024, 57, 11085−11096

Scheme 1. Synthetic Route to Obtain PI-Im-6FDA and PI-Im(Me)-6FDA

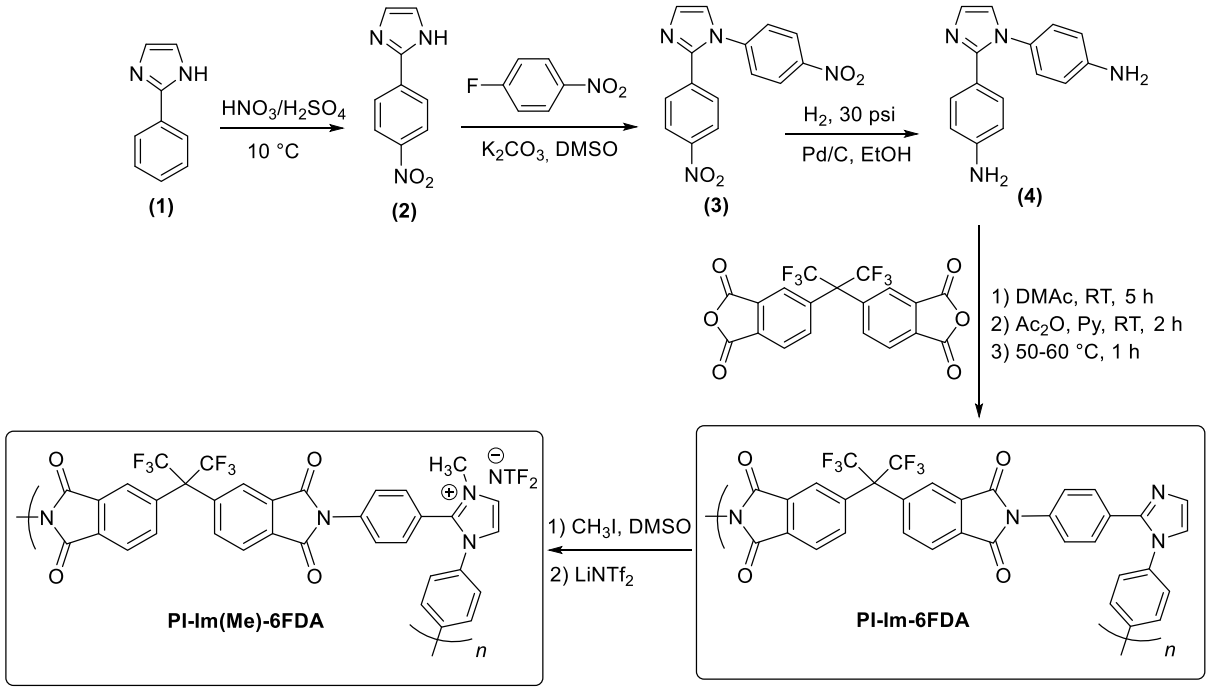

monomers in which the repeating units carry either a cation or an anion. Poly(IL)s retain many advantageous properties of ILs, such as thermal and chemical stability, while also exhibiting the inherent benefits of polymers. This makes them attractive for various applications, including catalysis, electrochemistry, and gas separation.[12−14] Among the cations typically utilized to create Poly(IL)s, the imidazolium framework stands out as the most adaptable and customizable substrate, given that it offers up to five sites for potential functionalization or derivatization.[15]

Poly(IL)s are predominantly synthesized through conventional free radical polymerization (FRP) of monomers containing double bonds, with step-growth polymerization being less commonly employed.[16−18] However, certain Poly(IL)s are produced via polycondensation methods, such as polyurethane, via polyepoxide step-growth chemistry, or through the Menshutkin reaction.[13,19−21] Alternatively, Poly(IL)s can be derived from custom-made polymers through postfunctionalization processes, which often involve ionization, quaternization, sulfation, or cross-linking of neutral polymer precursors.[22−25]

Ionenes containing a PI backbone (ionic PI) have been reported by several authors. For instance, Xu et al. reported the synthesis of copolyimides containing a benzimidazole moiety in the backbone, which were postfunctionalized using quaternization methods.[23] Their approach resulted in highly permeable and selective copolyimide membranes, showing great potential for CO_2/CH_4 or CO_2/N_2 gas separation. They also found that ionic copolyimides containing the $[Tf_2N]^-$ anion exhibited a better gas separation performance than those containing $[BF_4]^-$.

Li et al. investigated the synthesis of a random copolyimide by reacting 6FDA with both 4,4′-methylenedianiline (MDA) and diamino-imidazolium ILs.[26] The resulting ionic copolyimide had a low number-average molecular weight (M_n = 2.900), leading to poor thermal and mechanical properties. To address this issue, the same authors synthesized block copolyimides using the same monomers, achieving higher molecular weight values (M_n = 6.500) that allowed for the preparation of self-standing films. They found that gas *P* gradually decreased as the proportion of the imidazolium IL moiety increased, with CO_2 permeabilities ranging from 7 to 15 Barrer.

Kammakakam et al. reported the synthesis of a 6FDA/durene-based PI with pendant imidazolium cations.[27] This method involves modifying and converting one or more of the aryl methyl (i.e., Ar−CH_3) groups in the durene moiety into a benzylic bromide (i.e., Ar−CH_2Br), and then reacting a poly(ethylene glycol) (PEG)-functionalized imidazole with the polymer to create the pendant imidazolium cation. Chen et al. employed a similar modification strategy.[28] In their approach, a PI is first synthesized from 2,2′,6,6′-tetraphenyl-4,4′-oxidianiline (4-PhODA) and 6FDA monomers, followed by chloromethylation using paraformaldehyde with Me_3SiCl/$SnCl_4$ to introduce reactive sites on one or more of the pendant benzene rings. These benzylic chlorides are then reacted with 1-methylimidazole to form the pendant imidazolium cation, which is subsequently converted from $[Cl]^-$ to $[H_2PO_4]^-$. Bara et al. developed a versatile synthetic methodology for ionic PI containing the imidazolium within the backbone by preparing first an imidazole-terminated diimide monomer from two equiv of amine-functionalized imidazole and a dianhydride.[29] The diimidazole monomer was then reacted with a dihalide via a Menshutkin reaction, giving rise to ionic PIs containing two imidazolium cations within the repeating unit. The ionic PI membrane showed very low permeabilities for all gases tested. However, when 1-butyl-3-methylimidazolium bistriflimide ($[C_4mim][Tf_2N]$) was used as a "free" IL and mixed with the ionic PI, an increase in *P* was observed. The authors found that increases in gas diffusivity were responsible for the increased *P*.

To date, there are only a few reports of PIs containing neutral imidazole in their backbone. The above studies have described the formation of copolyimides using monomers with

https://doi.org/10.1021/acs.macromol.4c02315
Macromolecules 2024, 57, 11085−11096

benzimidazole or imidazolium cations, postfunctionalized PIs where imidazolium cations were present as pendant groups, or PIs with imidazolium cations formed during the polymerization process (i.e., the Menshutkin reaction). Our work aims to expand knowledge on the synthesis of PIs incorporating neutral imidazole rings along the polymer chain, which can then be postfunctionalized via quaternization reaction. We evaluate how the presence of ionic regions within the material affects the gas transport properties. The synthesis of PIs through polycondensation allows for the achievement of high molecular weights, which is beneficial for the formation of self-standing membranes.

In this work, a new diamine monomer containing an imidazole ring was synthesized through a three-step process: nitration of 2-phenyl-1*H*-imidazole, nucleophilic aromatic substitution of the resulting product with 4-nitro-1-fluorobenzene, and catalytic reduction of both nitro groups to amines (Scheme 1). The new diamine then reacted with 6FDA via polycondensation to produce a novel PI containing an imidazole ring, which was quaternized using methyl iodide, followed by exchanging $[I]^-$ for $[Tf_2N]^-$. All precursors, monomers, and polymers were extensively characterized, and their gas transport properties were evaluated.

Additionally, a systematic and cost-effective macromolecular packing model was generated using the *Polymatic* simulated polymerization algorithm,[30] which includes a compression/decompression scheme applied to the amorphous periodic unit cell. These models facilitated the estimation of key properties, such as density and FFV.

RESULTS AND DISCUSSION

Synthesis and Characterization of Precursors, Monomers, and Polymers. The precursors, monomers, and polymers are synthesized according to Scheme 1. Compound **2** was synthesized using a previously reported method from the literature,[31] resulting in a moderate yield of 77%. The successful isolation of compound **2** is highly dependent on controlling both the pH and the reaction temperature. At a low pH range (1−2) and temperatures below 10 °C, a yellow solid of the protonated version of compound **2** is formed. This solid subsequently dissolves with an increase in the temperature. Increasing the pH by using NaOH assists the precipitation of a yellow-green solid, which can then be isolated through filtration. This method highlights the importance of precise conditions in the synthesis and isolation process. Further, compound **2** undergoes a nucleophilic aromatic substitution reaction with 1-fluoro-4-nitrobenzene, yielding compound **3** with an 85% conversion rate. Subsequently, the dinitro compound is reduced in a H_2 atmosphere using Pd/C as a catalyst, followed by recrystallization, resulting in off-white diamine monomer **4** with a remarkable (95%) yield.

The structural characterization of compounds **2**, **3**, and **4** was investigated by using ATR-IR and NMR spectroscopy. Figure 1 displays the FT-IR spectrum of intermediate compounds. The compound **2** exhibited broad bands ranging from 3300 and ∼2200 cm^{-1}, corresponding to the stretching of N−H and C_{Im}−H (sp^2-H) bonds in the imidazole ring. Additionally, the presence of $-NO_2$ groups in compounds **2** and **3** is confirmed by absorption bands around 1500 and 1330 cm^{-1}, which are characteristic of symmetrical and asymmetrical stretching, respectively. For compound **4**, the N−H stretching bands observed between 3480−3320 cm^1, along with specific

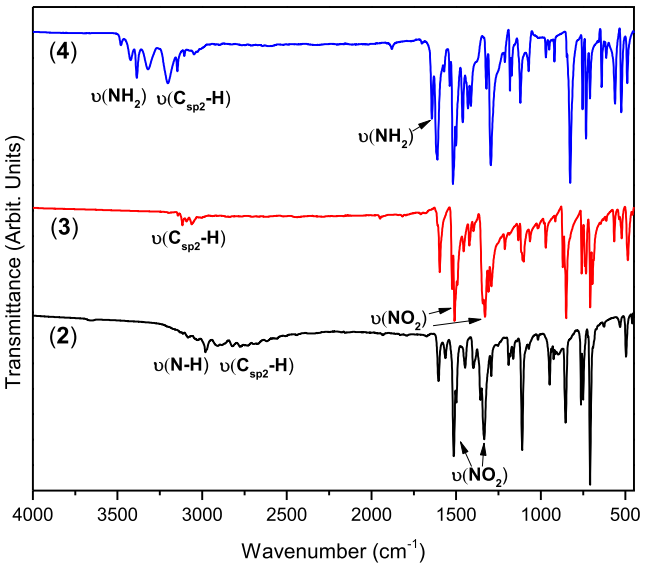

Figure 1. ATR-IR spectra of the precursors (**2** and **3**) and monomer (**4**).

N−H bending bands at 1644 and 1613 cm^{-1}, indicate the presence of amino groups.

The ^{1}H NMR spectrum of compound **2** (Figure S2) displays distinctive signals, including one at 12.97 ppm attributed to H8 (Im_{N-H}). Additionally, it exhibits signals at 8.32 and 8.18 ppm, which are associated with a *para*-substituted aromatic systems (H2 and H3), with a coupling constant of 9.0 Hz. A singlet observed at 7.29 ppm integrating for two protons, H6 and H7, which share the same chemical shift due to the well-known resonance effect of the imidazole ring, making a symmetrical magnetic environment for this molecule. Compounds **3** and **4** display a more complex pattern with multiple doublets in the ^{1}H NMR spectra (Figures S4 and S6) indicative of the structural complexity added by a second aromatic ring. This addition disrupts the symmetry observed in compound **2**, leading to a distinct separation of signals for hydrogens H6 and H7. These are observed as doublets with coupling constants of 1.3 Hz, reflective of their proximity to neighboring hydrogens in a five-membered ring context. The distinction between the spectra of compounds **3** and **4** is primarily marked by their chemical shifts, which are influenced by the presence of electron-withdrawing and electron-donating groups. Specifically, compound **3** exhibits signals at downfield positions due to a nitro group's electron-withdrawing effect, whereas signals for compound **4** are found at upfield positions, attributed to the electron-donating nature of an amino group. Additionally, unique singlets at 5.35 and 5.24 ppm are notable for the protons of the amino groups in compound **4**, each situated in a uniquely different magnetic environments. The ^{13}C NMR spectra (Figures S3, S5, and S7) further complement these findings by confirming the anticipated number of carbon atoms for each compound, providing a cohesive view of their molecular structures.

The PI, **PI-Im-6FDA**, was synthesized using a two-step method with a conventional low temperature, achieving 100% conversion of the starting material. This approach entailed reacting the readily available 6FDA with diamine **4** in DMAc solvent, initially forming polyamic acid. Subsequently, chemical cyclization was induced using pyridine and acetic anhydride as catalysts. For the preparation of the ionic PI, **PI-Im(Me)**-

https://doi.org/10.1021/acs.macromol.4c02315
Macromolecules 2024, 57, 11085−11096

6FDA, the procedure began with the reaction of **PI-Im-6FDA** with CH_3I in DMSO. This was followed by substituting the iodide ion with the Tf_2N anion, completing the synthesis process.

Figure 2 shows ATR-IR spectroscopy for **PI-Im-6FDA** and **PI-Im(Me)-6FDA**. The presence of imide groups is confirmed by the sharp absorption bands around 1780 and 1720 cm^{-1}, which are characteristic of the C═O stretching vibrations in the imide functionality. Additionally, the aromatic C═C stretch observed at 1608, 1517, and 1462 cm^{-1} alongside C_{Im}−H and C−H phenyl stretches at 3112 and 3068 cm^{-1}, respectively, underscores the aromatic nature of the polymer.

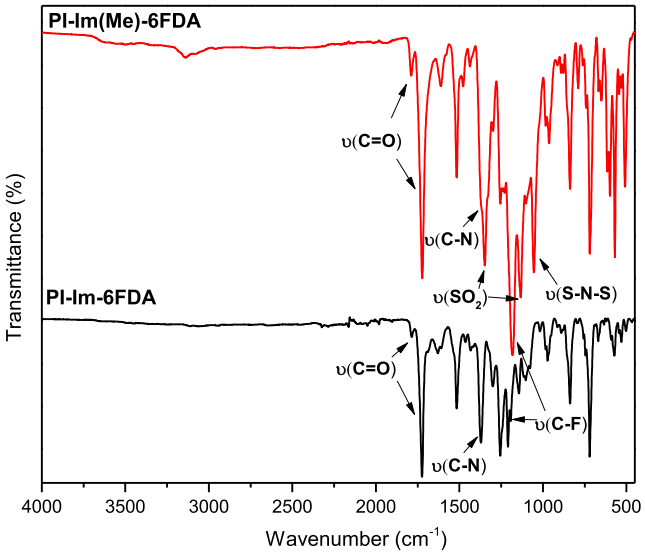

Figure 2. ATR-IR spectra of **PI-Im-6FDA** and **PI-Im(Me)-6FDA**.

The C−F stretch at 1193 cm^{-1} and the bending of the imide ring at 719 cm^{-1} further confirm the chemical structure of **PI-Im-6FDA**. On the other hand, **PI-Im(Me)-6FDA** distinguishes itself by the presence of additional bands at 2960 cm^{-1}, indicative of C−H aliphatic stretches, and notably, the S−N−S stretching at 1053 cm^{-1} and SO_2 stretching at 1349 and 1131 cm^{-1}. These features suggest the successful modification of **PI-Im-6FDA** with an ionic group, likely through the introduction of methyl iodide followed by anion exchange to incorporate the Tf_2N group, as inferred from the presence of the SO_2 and S−N−S vibrations. The maintenance of the C−F stretch, now at 1183 cm^{-1}, alongside the consistent bending of the imide ring at 719 cm^{-1}, validates the structural integrity of the PI framework postmodification. However, the complete methylation of every imidazole ring embedded in the PI backbone cannot be conclusively confirmed.

Figure 3 shows the ^1H NMR spectra of **PI-Im-6FDA** and **PI-Im(Me)-6FDA**. A similar pattern of signals belonging to the aromatic regions is observed in both PI, except for hydrogens H6 and H7, which were shifted to low field in **PI-Im(Me)-6FDA** due to the presence of the positive charge on

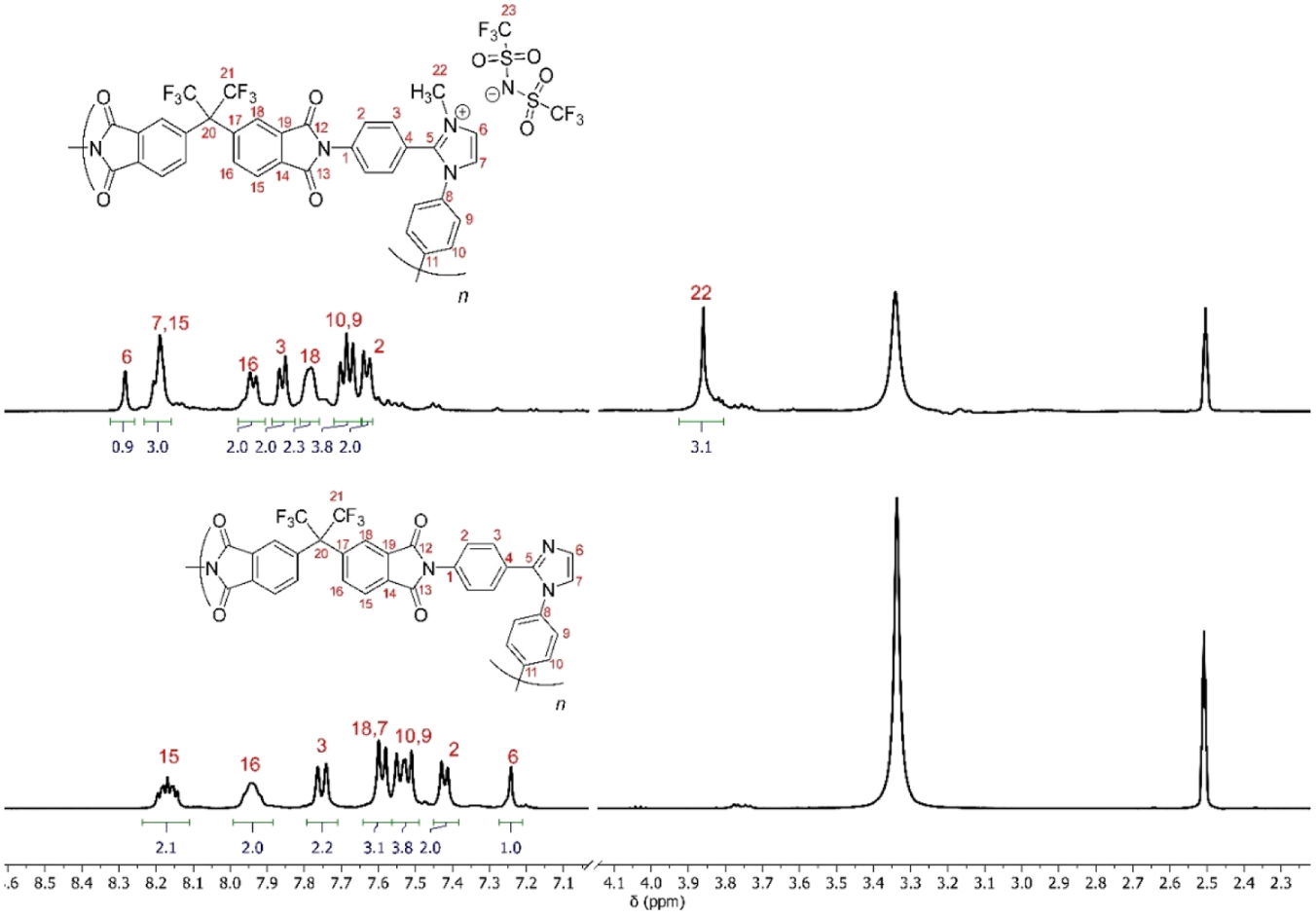

Figure 3. ^1H NMR spectra of **PI-Im-6FDA** and **PI-Im(Me)-6FDA**.

https://doi.org/10.1021/acs.macromol.4c02315
Macromolecules 2024, 57, 11085−11096

Table 1. Solubility of PI-Im-6FDA and PI-Im(Me)-6FDA in Various Common Organic Solvents and Their Number-Average Molecular Weight as Determined by MALDI-TOF Spectrometry

polymer	M_n (kDa)[a]	solubility[b]								
		DMF	DMAc	DMSO	NMP	$CHCl_3$	THF	acetone	alcohols[c]	water
PI-Im-6FDA	91	+	+	+	+	+	+	−	−	−
PI-Im(Me)-6FDA	84	+	+	+	+	−	−	+	−	−

[a]Number-average molecular weight. [b]Solubility test: 10 mg of sample in 1 mL of solvent. + Soluble at room temperature, −: insoluble even on heating until refluxing. [c]Methanol; ethanol; and 2-propanol.

the imidazole ring, altering the electronic density and therefore the observed chemical shift. Moreover, the peak at 3.86 ppm evidenced the presence of a methyl group in the structure of the ionic-PI.

In terms of ^{13}C NMR (Figures S8 and S9), both compounds display a wide range of chemical shifts reflecting the diversity of carbon environments. However, the presence of a carbon at 36.55 ppm in **PI-Im(Me)-6FDA** is characteristic of a methyl group, again supporting the aforementioned structural modification.

Finally, the ^{19}F NMR analysis for both compounds reveals chemical shifts at −62.87 and −62.85 ppm for F-6FDA, indicating a similar environment for this fluorine in both compounds. However, **PI-Im(Me)-6FDA** shows an additional shift at −78.74 ppm (F-Tf_2N), suggesting the introduction of a new fluorinated environment likely associated with the incorporation of this anion (Figures S10 and S11).

Solubility and Molecular Weight. Table 1 shows the solubility (S) behavior and molecular weight obtained from MALDI-TOF for both polymers. According to the table, the S results for **PI-Im-6FDA** and **PI-Im(Me)-6FDA** provide intriguing insights following the modification of the PI structure with ionic pendants. **PI-Im-6FDA** shows S in DMF, DMAc, DMSO, NMP, $CHCl_3$, and THF, but it is insoluble in acetone and alcohols. This pattern suggests that its S is favored in polar aprotic solvents, which can better solvate the rigid, aromatic, and nonionic structure of the polymer. The lack of S in acetone and alcohols could be attributed to the inability of these solvents to effectively disrupt the strong charge transfer complex among the imide groups.

PI-Im(Me)-6FDA, which contains ionic chains with a bulky Tf_2N anion within its structure, shows a distinct S profile. It is soluble in DMF, DMAc, DMSO, and NMP but insoluble in $CHCl_3$, THF, and alcohols while notably being soluble in acetone. This adjusted S profile can be explained by the presence of high ionic content in the backbone of **PI-Im(Me)-6FDA,** which enhances its S in polar aprotic solvents, including acetone with a polarity index[32] of 5.1, and decreases its S in less polar solvents like $CHCl_3$ (polarity index = 4.1) and THF (polarity index = 4.0). In addition, many authors have reported that the Tf_2N anions improve the S of the polymers in polar solvents, such as acetone.[33,34] On the other hand, the overall hydrophobic character due to the presence of aromatic rings and $-CF_3$ groups of both PI might reduce its S in highly polar solvents like water and alcohols.

The molecular weight results obtained by MALDI-TOF spectrometry for **PI-Im-6FDA** and **PI-Im(Me)-6FDA** are shown in Table 1 and Figure 4, indicating that both polymers possess high number-average molecular weights (M_n), with values of 91 and 84 kDa, respectively. These elevated molecular weights suggest that both polymers have substantial polymeric chain lengths.

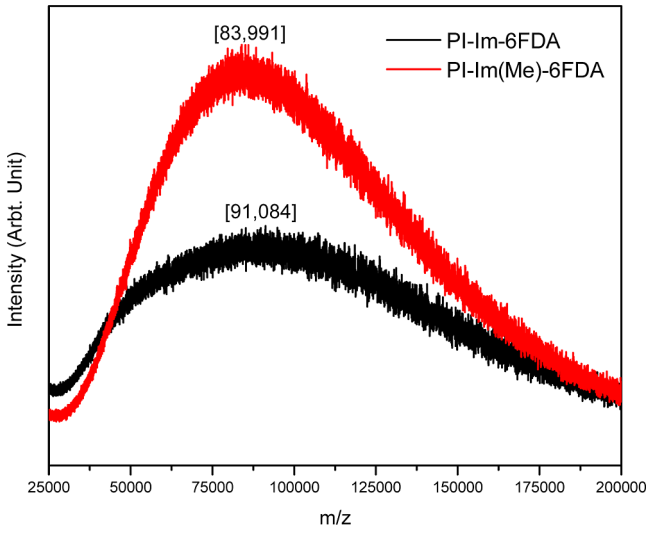

Figure 4. MALDI-TOF curves for **PI-Im-6FDA** and **PI-Im(Me)-6FDA**.

Wide-Angle X-ray, Thermal, and Mechanical Properties. Figure 5 displays the thermograms from TGA analyses for each polymer sample, including **PI-Im(Me)-6FDA + IL**, while Table 2 summarizes the data. It is evident that polymers exhibit significant thermal stability, with a 10% weight loss occurring at temperatures exceeding 400 °C. This notable thermal resistance primarily stems from the high aromatic content in these materials and the interactions formed by charge transfer complexes among the polymer chains.[35,36]

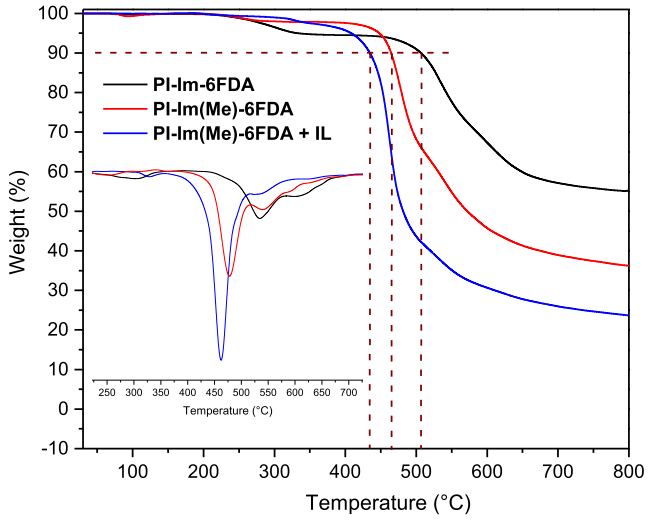

Figure 5. TGA and DTG (inside) plots for **PI-Im-6FDA**, **PI-Im(Me)-6FDA**, and **PI-Im(Me)-6FDA + IL**.

https://doi.org/10.1021/acs.macromol.4c02315
Macromolecules 2024, 57, 11085−11096

Table 2. Thermal and Mechanical Properties and *d*-Spacing Values for PI-Im-6FDA, PI-Im(Me)-6FDA, and PI-Im(Me)-6FDA + IL

polymer	T_{onset} (°C)[a]	$T_{10\%}$ (°C)[b]	R_w (%)[c]	T_g (°C)[d]	d-spacing (Å)[e]	tensile strength (MPa)	elongation at break (%)	Young's modulus (GPa)
PI-Im-6FDA	465	510	55	315	4.7−2.8	110.40	5.25	2.23
PI-Im(Me)-6FDA	420	465	36	315	3.7−2.9	n. d.	n. d.	n. d.
PI-Im(Me)-6FDA + IL	395	435	23	315	3.8	85.15	10.35	1.86

[a]Temperature at which the decomposition begin. [b]Temperature at which 10% weight is lost. [c]Residual weight carbon (char). [d]Glass transition temperature recorded at a heating rate of 50 °C min^{-1}. [e]Distance between chains.

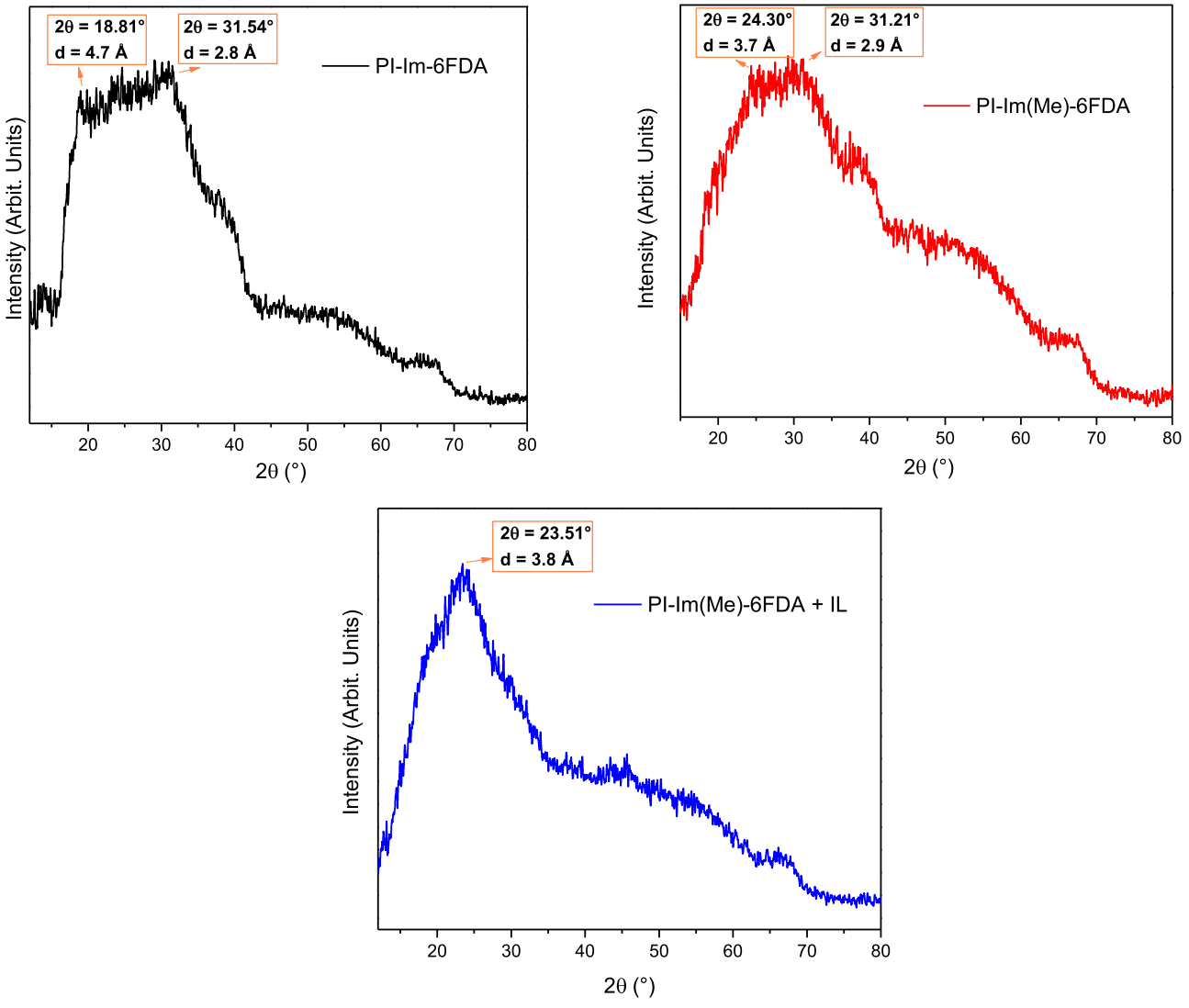

Figure 6. Diffractograms for each sample.

However, **PI-Im(Me)-6FDA** and **PI-Im(Me)-6FDA + IL** display lower onset temperatures (T_{onset}) and $T_{10\%}$ values, which are related to the presence of the Tf_2N anion, known to start degrading at temperatures around 400 °C, as previously reported.[37] In our study, the T_{onset} values for these two samples were 420 and 395 °C, respectively. Furthermore, an increased Tf_2N content is expected to lead to greater mass loss, aligning with our R_w data, where the sample containing IL exhibits a higher amount of this anion.

A DSC experiment was conducted on each sample, from 25 to 350 °C at a rate of 10 °C per minute, to determine the glass transition temperatures (T_g). However, T_g was not detected in any of the samples at this heating rate. This result is not surprising, as it is well-known that when polymer chains are highly rigid, the T_g is often not observed in many PIM family polymers.[38] However, when the measurement was conducted at 50 °C min^{-1} it was possible to see a transition around 315 °C for each sample. The presence of ionic regions along the main polymer chain in **PI-Im(Me)-6FDA**, as well as of IL in **PI-Im(Me)-6FDA + IL**, does not significantly affect the T_g values, suggesting that the polymer chain's stiffness remains unchanged compared to the pristine PI. However, the elevated T_g values obtained are primarily attributed to the presence of bulky $-CF_3$ groups and the rigid 1,2-substitution on the imidazole ring, which increase the stiffness of the main chain.

https://doi.org/10.1021/acs.macromol.4c02315
Macromolecules 2024, 57, 11085−11096

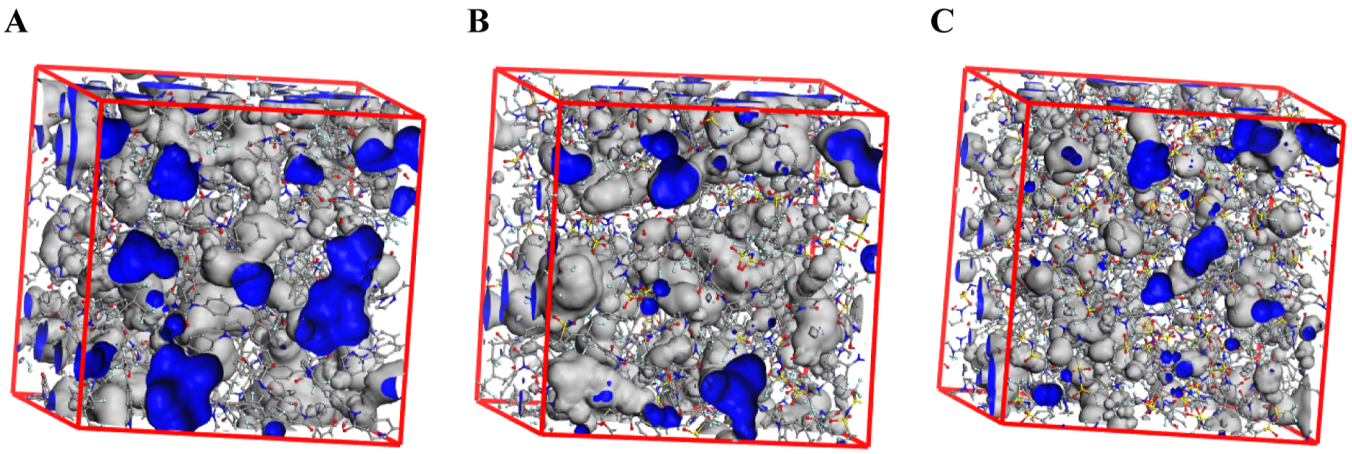

Figure 7. Unit cell representation of a simulated polymer representative of (A) **PI-Im-6FDA**, (B) **PI-Im(Me)-6FDA**, and (C) **PI-Im(Me)-6FDA + IL**.

Mechanical properties were measured only for **PI-Im-6FDA** and **PI-Im(Me)-6FDA + IL** because the **PI-Im(Me)-6FDA** sample was brittle. As can be seen in Table 2, **PI-Im-6FDA** shows a higher tensile strength of 110.4 MPa but a lower elongation at break (6.66%) compared to **PI-Im(Me)-6FDA + IL**, which has a tensile strength of 85.15 MPa and a higher elongation at break (10.35%). The Young's modulus of both samples was ∼2 GPa. The higher elongation at break seen in **PI-Im(Me)-6FDA + IL** could be attributed to the presence of IL in the film, which acts as a lubricant between the polymer chains.

The diffractogram in Figure 6 shows the diffraction peaks obtained for all samples. The presence of broad and poorly defined peaks confirms the amorphous structure of these materials due to the chains can be arranged randomly and without a repetitive pattern.[39] However, it is interesting to observe how the main halo becomes increasingly narrow as the presence of ionic regions in the main chain increases, becoming more defined in the sample containing IL. Probably, IL increases the intermolecular interaction between main-chain and free IL.

The distance between chains was calculated by the *d*-spacing parameter in Bragg's law (Table 2), corresponding to the maximum in the amorphous WAXD halo. The results were 4.7−2.8 Å for **PI-Im-6FDA**, 3.7−2.9 Å for **PI-Im(Me)-6FDA**, and 3.8 Å for **PI-Im(Me)-6FDA + IL**. Evidently, an increase in ionic content within the main chain enhances electrostatic interactions, prompting the chains to draw nearer to each other. This proximity among the chains consequently leads to a decrease in the *d*-spacing.

Computational Simulation. Figure 7 shows a unit cell under periodic conditions for each simulated polymer. The surface viewed from the interior of the cavities is colored blue, while its exterior is represented in gray. This representation visualizes that the polymer model **PI-Im-6FDA** generates more cavities per unit cell than polymers **PI-Im(Me)-6FDA** and **PI-Im(Me)-6FDA + IL**. Table 3 presents the averaged values of the simulated density (Sim. density) and FFV (calculated according to the Connolly surface with a probe radius of 1.65 Å), based on the results obtained from the ten representative computational models of each polymer. This table also includes the experimental density values (Exp. density) for comparison.

Table 3. Experimental and Simulated Density and Calculated FFV for PI-Im-6FDA, PI-Im(Me)-6FDA, and PI-Im(Me)-6FDA + IL

polymer	Exp. density (g cm^{-3})	Sim. density (g cm^{-3})	FFV
PI-Im-6FDA	1.2381 ± 0.0061	1.2192 ± 0.0125	0.145 ± 0.015
PI-Im(Me)-6FDA	1.3742 ± 0.0053	1.3215 ± 0.0125	0.118 ± 0.012
PI-Im(Me)-6FDA + IL	1.4243 ± 0.0086	1.3663 ± 0.0179	0.075 ± 0.014

Analysis of the density values reveals that the results obtained from the computational models follow the same trend as the experimental ones, although with lower values. As the ionic content increases, due to either the quaternization process experienced by **PI-Im-6FDA** or the addition of IL to this ionic PI, the density value also increases. This is attributed to a greater compaction of the polymeric structure due to electrostatic attraction between the chains. As expected, the FFV decreases progressively with increasing ionic content.

Gas Transport Properties. As was described in the experimental section, dense films were prepared from each sample. However, the **PI-Im(Me)-6FDA** film was quite brittle, and it was not possible to conduct gas permeation measurements for this sample. This poor self-standing behavior seen for this sample may be due to multiple factors. Quaternization of imidazole, for instance, altered the structural order of the polymer chains, which might reduce the ductility of the material. This is evident from the WAXD data. Another factor likely could be incomplete quaternization of the imidazole rings in the pristine PI, which could result in incompatibility/repulsions between the quaternized and neutral chains. This might create microdomains that act as stress concentration points, facilitating material fracture under deformation.[40] Indeed, when the IL is added to **PI-Im(Me)-6FDA**, the film again exhibits good self-standing behavior, most likely because the IL is acting as a plasticizer, enhancing the intermolecular interactions of the polymer chains, validated from the *d*-spacing and density values.

Table 4 presents the gas *P*, ideal selectivity (α), diffusion (D), and S coefficients, along with the diffusion-selectivity (D_i/D_j) and solubility-selectivity (S_i/S_j) for **PI-Im-6FDA** and **PI-Im(Me)-6FDA + IL**. As can be seen, for **PI-Im-6FDA**, the *P* decreases as the kinetic radius of the gas increases [H_2 (2.89

https://doi.org/10.1021/acs.macromol.4c02315
Macromolecules 2024, 57, 11085−11096

Table 4. PI-Im-6FDA and PI-Im(Me)-6FDA + IL Films Pure Gas Permeability, Diffusion, and Solubility Coefficients, and Gas Pair Ideal Gas Selectivity Results at 35 °C and 2 Bar Upstream Pressure

membrane	permeability P_i (Barrer)[a]					ideal selectivity α (P_i/P_j)			
	H_2*	O_2	N_2	CH_4	CO_2	H_2/N_2	O_2/N_2	CO_2/CH_4	CO_2/N_2
PI-Im-6FDA	20.05	2.83	0.58	0.65	19.62	34.56	4.87	30.18	33.82
PI-Im(Me)-6FDA + IL	9.60	2.42	0.77	0.99	17.52	12.22	3.14	17.69	22.75
membrane	diffusion D_i[b]				solubility S_i[c]				
	O_2	N_2	CH_4	CO_2	O_2	N_2	CH_4	CO_2	
PI-Im-6FDA	3.34	0.62	0.34	1.22	0.86	0.94	1.91	16.08	
PI-Im(Me)-6FDA + IL	6.66	5.17	2.87	3.40	0.36	0.15	0.34	5.15	
membrane	diffusion-selectivity (Di/Dj)			solubility-selectivity (Si/Sj)					
	O_2/N_2	CO_2/CH_4	CO_2/N_2	O_2/N_2	CO_2/CH_4	CO_2/N_2			
PI-Im-6FDA	5.38	3.58	1.96	0.91	8.41	17.11			
PI-Im(Me)-6FDA + IL	1.28	1.18	0.65	2.40	15.14	34.33			

[a]Barrer = 10^{-10} cm^3 (STP) cm cm^{-2} s^{-1} cm Hg^{-1}. [b]Diffusion coefficient ($D \times 10^{-8}$) cm^2 s^{-1}. [c]Solubility coefficient ($S \times 10^{-2}$) cm^3 (STP) cm^3 cm Hg. *The values of D and S for H_2 are not shown due to the rapid attainment of steady state for this gas.

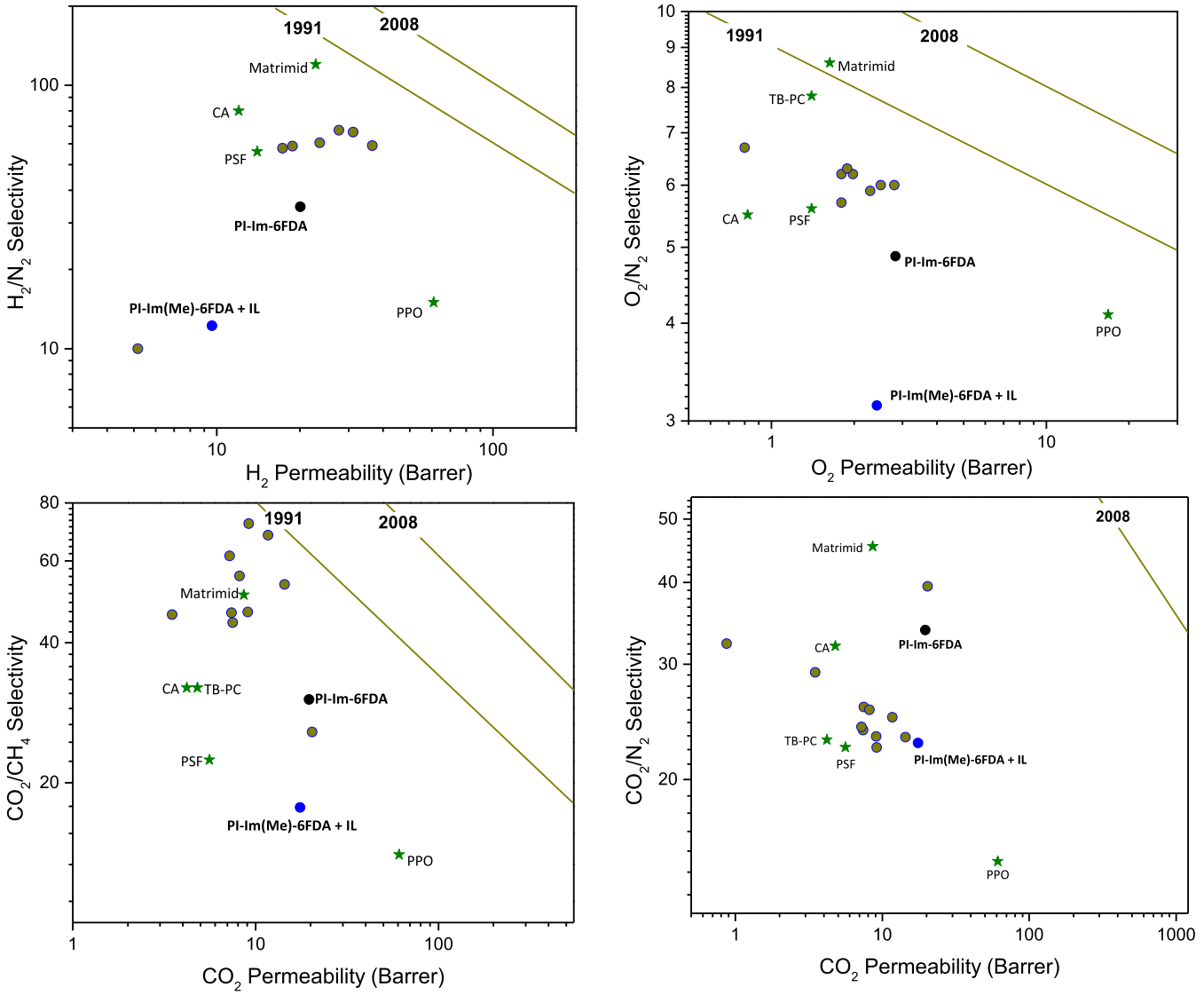

Figure 8. Robeson plots for gas pairs H_2/N_2, O_2/N_2, CO_2/CH_4, and CO_2/N_2. (Green stars) Commercial membranes. (Gray circles with blue border) Membranes that contain imidazolium in the main polymer chain or as a side group. (Black circle) **PI-Im-6FDA.** (Blue circle) **PI-Im(Me)-6FDA + IL.**

https://doi.org/10.1021/acs.macromol.4c02315
Macromolecules 2024, 57, 11085−11096

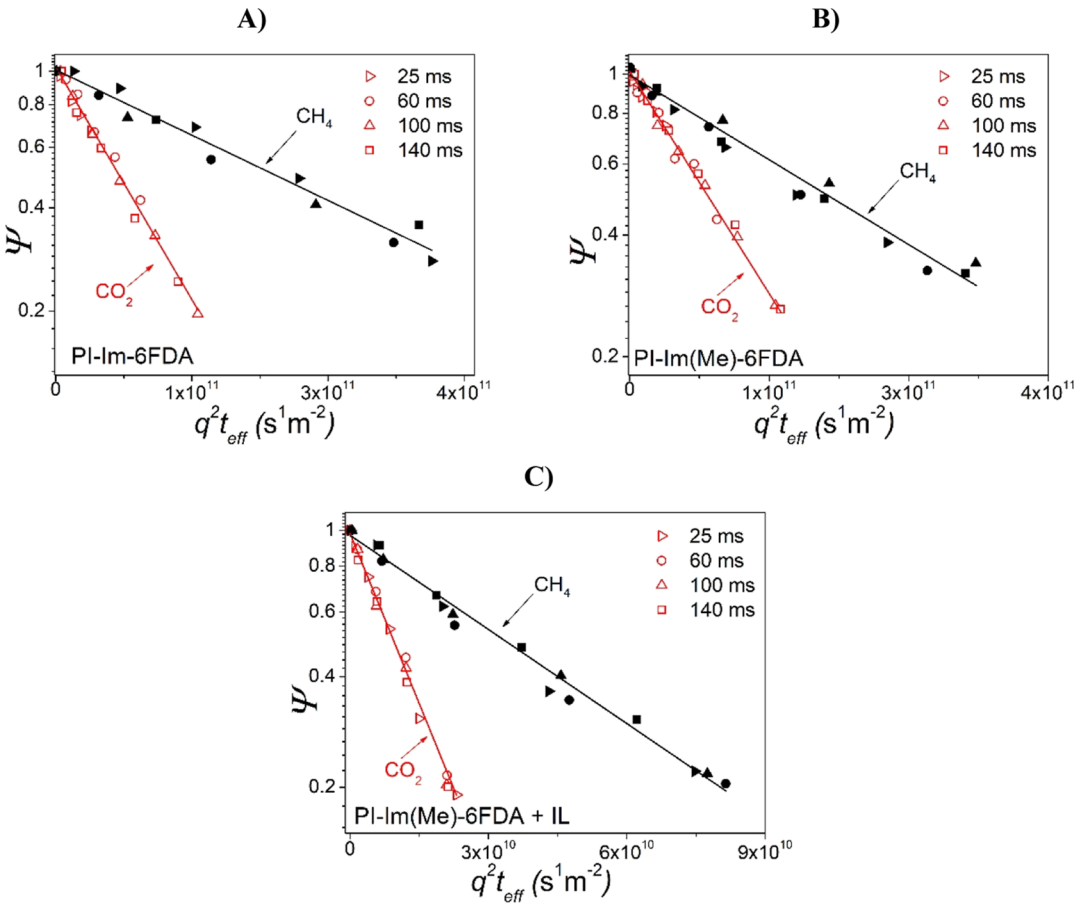

Figure 9. PFG NMR attenuation plots measured at 80 °C in (A) **PI-Im-6FDA**, (B) **PI-Im(Me)-6FDA**, and (C) **PI-Im(Me)-6FDA** + IL polymer membranes loaded with CO_2 (hollow, red points) or CH_4 (filled, black points). Straight lines represent best fit lines using eq S6 (see Supporting Information). Symbol shape indicates the effective diffusion time.

Å), CO_2 (3.3 Å), O_2 (3.46 Å), N_2 (3.64 Å), CH_4 (3.8 Å)].[41,42] However, it is notable that this order changes for **PI-Im(Me)-6FDA + IL**, where CO_2 becomes the most permeable gas despite its larger kinetic radius compared to H_2. This is due to the strong dipolar−quadrupolar interactions between the ionic domains in the main chain and the CO_2 molecules.

Another interesting result is that for gases with smaller kinetic diameters (H_2, CO_2, and O_2), the *P* decreased in **PI-Im(Me)-6FDA + IL** compared to **PI-Im-6FDA,** with the most significant decrease observed for H_2. However, for larger gases such as N_2 and CH_4, the *P* was higher in **PI-Im(Me)-6FDA + IL.**

To understand this result, we can analyze the *D* and *S* coefficients. For all gases, in the sample containing IL, the *S* decreased while the *D* increased. However, the decrease in *S* for O_2 and CO_2 was 2.4 and 3.1 times, respectively, while the increase in *D* was 2 and 2.8 times for the same gas pair, respectively. Practically, for these pairs of gases, the loss in *S* was compensated by a corresponding increase in *D*. In the cases of N_2 and CH_4, *S* decreased by about six times for both gases (5.6 times for CH_4 and 6.3 times for N_2), while the increase in *D* was slightly higher, being 8.3 times for N_2 and 8.4 times for CH_4. Considering that the FFV decreased when moving from **PI-Im-6FDA** to **PI-Im(Me)-6FDA + IL**, it was expected that gas *D* through the membrane would also decrease. However, the result was the opposite. Evidently, the IL acts as a carrier for the gas through the chains, increasing its *D*. On the other hand, in the solution-*D* model, *S* is related to the sorption of the gas on the membrane surface. Therefore, the presence of IL on the surface hinders this process due to the significant difference between the IL (polar) and the tested gases (nonpolar).

PI-Im(Me)-6FDA + IL showed lower selectivity values than **PI-Im-6FDA** for all pairs of gases. According to eq S5 (see Supporting Information), the α can be expressed as a function of S_i/S_j and D_i/D_j. The results for the separation of gas mixtures O_2/N_2, CO_2/CH_4, and CO_2/N_2 demonstrate that the differences in the α values exhibited by the membranes are due to the fact that the decrease in D_i/D_j is more pronounced when moving from **PI-Im-6FDA** to **PI-Im(Me)-6FDA + IL,** compared to the corresponding increase in S_i/S_j values, respectively. It is important to note that it was previously indicated that *D* increased and *S* decreased when moving from **PI-Im-6FDA** to **PI-Im(Me)-6FDA + IL,** which is related to the *P* results. However, what is being discussed now pertains to the differences in the selectivity results.

Based on the data from Table 4, Robeson plots were also created and are shown in Figure 8 for the gas pairs H_2/N_2, O_2/N_2, CO_2/CH_4, and CO_2/N_2. In these diagrams, each material is represented by a point that indicates its α for separating a mixture of two gases in relation to the *P* of the membrane to the gas that permeates through it most rapidly. For comparison, the diagrams also display data from five other commercially available membranes used for gas separation: Matrimid, CA, tetrabromobisphenol A polycarbonate (TB-PC), polysulfone (PSF), and PPO.[43,44] These are depicted

https://doi.org/10.1021/acs.macromol.4c02315
Macromolecules 2024, 57, 11085−11096

Table 5. Self-Diffusion Data Obtained from the Measured PFG NMR Attenuation Curves at 80 °C[a]

sample	sorbate	range of t_{eff} (ms)	Ds × 10^7 (cm^2/s)	range of RMSDs (μm)	diffusion-selectivity ($D_{s_{CO_2}}/D_{s_{CH_4}}$)[b]
PI-Im-6FDA	CO_2	25−140	1.1 ± 0.1	1.4 ± 0.1−3.2 ± 0.3	3.04
	CH_4	25−140	0.37 ± 0.04	0.8 ± 0.1−1.9 ± 0.2	
PI-Im(Me)-6FDA	CO_2	25−140	0.98 ± 0.09	1.2 ± 0.1−2.9 ± 0.3	2.62
	CH_4	25−140	0.37 ± 0.04	0.8 ± 0.1−1.8 ± 0.2	
PI-Im(Me)-6FDA + IL	CO_2	25−140	7.1 ± 0.7	3.3 ± 0.3−7.8 ± 0.8	3.61
	CH_4	25−140	1.9 ± 0.2	1.8 ± 0.2−3.8 ± 0.4	

[a]RMSDs were calculated using eq S7 (see Supporting Information) [b]20% experimental uncertainty.

with a green star. Gray circles with blue borders represent membranes that contain imidazolium in the main polymer chain or as a side group.[26,29]

The performance evaluation of the membranes developed in this study can be conducted by analyzing their positions (P_i, $\alpha_{i,j}$) on each Robeson plot in comparison with the other membranes. The permeabilities of **PI-Im-6FDA** and **PI-Im(Me)-6FDA + IL** exceeded those of most commercial membranes, except for PPO and for the H_2/N_2 gas mixture. However, their selectivity performance was lower than that of most commercial membranes, adhering to the well-known trade-off between P and selectivity. For gas pairs involving CO_2, the best performances in terms of combined permselectivity properties were observed. Notably, **PI-Im-6FDA** showed particularly favorable results, as its position on the Robeson plots for CO_2/CH_4 and CO_2/N_2 was in the central region, indicating an acceptable balance between P and selectivity.

Gas Self-Diffusion by PFG NMR. Figure 9 shows the PFG NMR attenuation curves measured for CO_2 and CH_4 diffusing in **PI- Im-6FDA, PI-Im(Me)-6FDA,** and **PI-Im(Me)-6FDA + IL** membranes at 80 °C for effective D times ranging between 25 and 140 ms.

The monoexponential attenuation behavior (linear in the semilogarithmic presentation of Figure 9) was observed for all three membrane types. Any signal from the gas phase surrounding the membrane was attenuated away already at the smallest value of the magnetic field gradient amplitude used. As a result, the signal attenuation data in Figure 9 are attributed to gas molecules diffusing inside of the membranes. The data in Figure 9 are in agreement with eq S6 (see Supporting Information), thus indicating the absence of any distribution over gas self-diffusivities in each sample and the lack of a dependence of the intramembrane self-diffusivities on the effective D time and the corresponding RMSD values in the measured range. The values of self-D coefficients were obtained from the best fit lines using eq S6 (see Supporting Information), and the corresponding ranges of RMSDs were calculated using eq S7 (see Supporting Information). The results are shown in Table 5.

The smallest values of the RMSDs used in the measurements were around 1−2 μm for all membrane samples (Table 5). Hence, the reported PFG NMR data show that the membrane transport properties are uniform on the length scales ≥1−2 μm in each membrane. The self-D coefficients were observed to be around an order of magnitude larger in comparison with the reported macroscopic transport diffusivities. This difference is not surprising considering the significantly larger temperature used in the PFG NMR self-D measurements. As discussed above, the higher temperature of 80 °C was used in the PFG NMR self-D measurements due to the signal-to-noise limitations observed at the lower temperature of 35 °C, which was chosen for the macroscopic transport D measurements. The data in Table 5 show that the addition of the IL leads to a significant increase in the self-diffusivities of both gases. At the same time, the IL addition preserves the D_i/D_j of around 3, which was also observed for the other two membranes (Table 5).

CONCLUSIONS

The syntheses of **PI-Im-6FDA** and **PI-Im(Me)-6FDA** were successfully completed with high yields, and their structures were confirmed through ATR-IR and NMR techniques. MALDI-TOF analysis revealed that both polymers have a high molecular weight, indicating substantial polymeric chain lengths. The introduction of ionic groups in the backbone through the imidazole quaternization significantly altered the polymer properties, particularly S and molecular interactions between chains. The usage of a common IL, $[C_4mIm][Tf_2N]$, allowed the fabrication of a good self-standing film from **PI-Im(Me)-6FDA**, which was brittle, likely owing to the lack of amorphous regions. All three materials exhibited excellent thermal stability. The presence of ionic groups slightly decreased the thermal stability but still maintained high resistance to thermal decomposition. The simulated densities and FFV were consistent with experimental findings, showing an increase in density and a decrease in free volume with higher ionic content, suggesting enhanced chain packing due to electrostatic interactions. The gas P studies demonstrated that **PI-Im-6FDA** and **PI-Im(Me)-6FDA + IL** had performances in gas separation compared with various commercial membranes, particularly for CO_2. The IL modification improved the D of gases and adjusted the S and P characteristics, although it reduced the overall selectivity compared to the nonionic counterpart. The results from this study provide a comprehensive understanding of the structural, thermal, and gas transport properties of these imidazole and imidazolium-containing PIs, paving the way for their application in membrane technologies for gas separation. The results also demonstrate that membrane transport properties are uniform over length scales greater than or equal to 1−2 μm, as evidenced by the PFG NMR self-D measurements performed over a range of D time and length scales. The significant increase in the gas self-diffusivities observed by PFG NMR with the addition of the IL further suggests that the IL enhances the membrane's gas transport capabilities while maintaining the self- D_i/D_j.

ASSOCIATED CONTENT

Supporting Information

The Supporting Information is available free of charge at https://pubs.acs.org/doi/10.1021/acs.macromol.4c02315.

https://doi.org/10.1021/acs.macromol.4c02315
Macromolecules 2024, 57, 11085−11096

Materials and methods, synthetic procedures, gas loading pressures inside the studied NMR samples, computational simulation, film preparation, monomer synthesis, and synthesis of polyimides (PDF)

AUTHOR INFORMATION

Corresponding Authors

Alain Tundidor-Camba − *Department of Chemical & Biological Engineering, The University of Alabama, Tuscaloosa, Alabama 35487-0203, United States;* orcid.org/0009-0002-8726-3606; Email: atundidorcamba@ua.edu

Jason E. Bara − *Department of Chemical & Biological Engineering, The University of Alabama, Tuscaloosa, Alabama 35487-0203, United States;* orcid.org/0000-0002-8351-2145; Email: jbara@eng.ua.edu

Authors

Sudhir Ravula − *Department of Chemical & Biological Engineering, The University of Alabama, Tuscaloosa, Alabama 35487-0203, United States;* orcid.org/0000-0002-3457-7102

Fidel E. Rodríguez-González − *Research Laboratory for Organic Polymers (RLOP), Department of Organic Chemistry, Pontificia Universidad Católica de Chile, Santiago 7820436, Chile*

Pravin S. Shinde − *Department of Chemical & Biological Engineering, The University of Alabama, Tuscaloosa, Alabama 35487-0203, United States;* orcid.org/0000-0002-1715-6867

Ana L. Montero-Alejo − *Departamento de Física, Facultad de Ciencias Naturales, Matemática y del Medio Ambiente (FCNMM), Universidad Tecnológica Metropolitana, Santiago 7800003, Chile;* orcid.org/0000-0003-1675-0546

Claudio A. Terraza − *Research Laboratory for Organic Polymers (RLOP), Department of Organic Chemistry, Pontificia Universidad Católica de Chile, Santiago 7820436, Chile; UC Energy Research Center, Pontificia Universidad Católica de Chile, Santiago 7820436, Chile*

Sree Laxmi − *Department of Chemical Engineering, University of Florida, Gainesville, Florida 32611, United States*

Sergey Vasenkov − *Department of Chemical Engineering, University of Florida, Gainesville, Florida 32611, United States*

Kathryn E. O'Harra − *Department of Chemical & Biological Engineering, The University of Alabama, Tuscaloosa, Alabama 35487-0203, United States;* orcid.org/0000-0001-5328-0024

Complete contact information is available at: https://pubs.acs.org/10.1021/acs.macromol.4c02315

Author Contributions

The manuscript was written-reviewed and edited through contributions of all authors. All authors have given their approval to the final version of the manuscript. S.R.: methodology and investigation. F.E.R-G.: validation and investigation. P.S.S.: methodology. A.L.M-A.: conceptualization and validation. C.A.T.: conceptualization and validation. S.L.: methodology and validation. S.V.: conceptualization, methodology, and validation. K.E.O.H.: conceptualization and methodology. A.T-C.: conceptualization, methodology, validation, and supervision. J.E.B.: conceptualization, validation, supervision, project administration, and funding acquisition.

Notes

The authors declare no competing financial interest.

ACKNOWLEDGMENTS

This material is based upon work supported by the U.S. Department of Energy, Office of Science, Office of Basic Energy Sciences, under Award no. DE-SC0025219. This work was funded by the Agencia Nacional de Investigación y Desarrollo through Fondecyt Regular project no. 1230077 and by the NSF (CBET award no. 2312001). A portion of this work was performed at the National High Magnetic Field Laboratory, which is supported by the National Science Foundation Cooperative Agreement no. DMR-2128556 and the State of Florida. Powered@NLHPC: this research was partially supported by the supercomputing infrastructure of the NLHPC (CCSS210001), Chile. This research was supported by the Cluster Faraday UTEM (CONICYT- FONDEQUIP—EQM180180), Chile.

REFERENCES

(1) Kim, S.; Lee, Y. M. Rigid and Microporous Polymers for Gas Separation Membranes. *Prog. Polym. Sci.* **2015**, *43*, 1−32.

(2) Budd, P. M.; McKeown, N. B. Highly Permeable Polymers for Gas Separation Membranes. *Polym. Chem.* **2010**, *1*, 63−68.

(3) Rodríguez, A.; Velázquez Tundidor, M. V.; Cruz, Y.; Rodríguez-González, F. E.; Aguilar-Vega, M. J.; Sulub-Sulub, R.; Ravula, S.; Bara, J. E.; Terraza, C. A.; Tundidor-Camba, A. Polyimides Containing Biphenyl and Tröger's Base Units for Gas Separation Membranes. *ACS Appl. Polym. Mater.* **2024**, *6* (6), 3342−3353.

(4) Ma, X.-H.; Yang, S.-Y. Polyimide Gas Separation Membranes. In *Advanced Polyimide Materials*; Elsevier, 2018; pp 257−322..

(5) Hossain, I.; Al Munsur, A. Z.; Choi, O.; Kim, T.-H. Bisimidazolium PEG-Mediated Crosslinked 6FDA-Durene Polyimide Membranes for CO2 Separation. *Sep. Purif. Technol.* **2019**, *224*, 180−188.

(6) Hossain, I.; Al Munsur, A.; Kim, T.-H. A Facile Synthesis of (PIM-Polyimide)-(6FDA-Durene-Polyimide) Copolymer as Novel Polymer Membranes for CO2 Separation. *Membranes* **2019**, *9* (9), 113.

(7) O'Harra, K.; Kammakakam, I.; Devriese, E.; Noll, D.; Bara, J.; Jackson, E. Synthesis and Performance of 6FDA-Based Polyimide-Ionenes and Composites with Ionic Liquids as Gas Separation Membranes. *Membranes* **2019**, *9* (7), 79.

(8) Qiu, W.; Xu, L.; Chen, C.-C.; Paul, D. R.; Koros, W. J. Gas Separation Performance of 6FDA-Based Polyimides with Different Chemical Structures. *Polymer* **2013**, *54* (22), 6226−6235.

(9) Tanaka, K.; Okano, M.; Toshino, H.; Kita, H.; Okamoto, K. Effect of Methyl Substituents on Permeability and Permselectivity of Gases in Polyimides Prepared from Methyl-substituted Phenylenediamines. *J. Polym. Sci., Part B: Polym. Phys.* **1992**, *30* (8), 907−914.

(10) Liu, Y.; Pan, C.; Ding, M.; Xu, J. Gas Permeability and Permselectivity of Polyimides Prepared from Phenylenediamines with Methyl Substitution at the Ortho Position. *Polym. Int.* **1999**, *48* (9), 832−836.

(11) Lin, W.-H.; Vora, R. H.; Chung, T.-S. Gas Transport Properties of 6FDA-Durene/1,4-Phenylenediamine (PPDA) Copolyimides. *J. Polym. Sci., Part B: Polym. Phys.* **2000**, *38* (21), 2703−2713.

(12) Chen, S.; Dong, Y.; Sun, J.; Gu, P.; Wang, J.; Zhang, S. Ionic Liquids Membranes for Liquid Separation: Status and Challenges. *Green Chem.* **2023**, *25* (15), 5813−5835.

(13) Friess, K.; Izák, P.; Kárászová, M.; Pasichnyk, M.; Lanč, M.; Nikolaeva, D.; Luis, P.; Jansen, J. C. A Review on Ionic Liquid Gas Separation Membranes. *Membranes* **2021**, *11* (2), 97.

(14) Bernardo, G.; Gaspar, H. Recent Advances in Poly(Ionic Liquid)-Based Membranes for CO2 Separation. *Polymers* **2023**, *15* (3), 667.
(15) Bara, J. E.; Shannon, M. S. Beyond 1,3-Difunctionalized Imidazolium Cations. *Nanomater. Energy* **2012**, *1* (4), 237−242.
(16) Bara, J. E.; Lessmann, S.; Gabriel, C. J.; Hatakeyama, E. S.; Noble, R. D.; Gin, D. L. Synthesis and Performance of Polymerizable Room-Temperature Ionic Liquids as Gas Separation Membranes. *Ind. Eng. Chem. Res.* **2007**, *46* (16), 5397−5404.
(17) Jangu, C.; Long, T. E. Phosphonium Cation-Containing Polymers: From Ionic Liquids to Polyelectrolytes. *Polymer* **2014**, *55* (16), 3298−3304.
(18) McDanel, W. M.; Cowan, M. G.; Carlisle, T. K.; Swanson, A. K.; Noble, R. D.; Gin, D. L. Cross-Linked Ionic Resins and Gels from Epoxide-Functionalized Imidazolium Ionic Liquid Monomers. *Polymer* **2014**, *55* (16), 3305−3313.
(19) Mori, D. I.; Martin, R. M.; Noble, R. D.; Gin, D. L. Cross-Linked, Polyurethane-Based, Ammonium Poly(Ionic Liquid)/Ionic Liquid Composite Films for Organic Vapor Suppression and Ion Conduction. *Polymer* **2017**, *112*, 435−446.
(20) Rembaum, A.; Noguchi, H. Reactions of N,N,N',N'-Tetramethyl-α,ι-Diaminoalkanes with α,ι-Dihaloalkanes. II. x-y Reactions. *Macromolecules* **1972**, *5* (3), 261−269.
(21) Noguchi, H.; Rembaum, A. Reactions of N,N,N',N'-Tetramethyl-α,ι-Diaminoalkanes with α,ι-Dihaloalkanes. I. 1-y Reactions. *Macromolecules* **1972**, *5* (3), 253−260.
(22) Nikolaeva, D.; Azcune, I.; Tanczyk, M.; Warmuzinski, K.; Jaschik, M.; Sandru, M.; Dahl, P. I.; Genua, A.; Loïs, S.; Sheridan, E.; Fuoco, A.; Vankelecom, I. F. J. The Performance of Affordable and Stable Cellulose-Based Poly-Ionic Membranes in CO2/N2 and CO2/CH4 Gas Separation. *J. Membr. Sci.* **2018**, *564*, 552−561.
(23) Xu, X.; Wang, J.; Dong, J.; Li, H.-B.; Zhang, Q.; Zhao, X. Ionic Polyimide Membranes Containing Tröger's Base: Synthesis, Microstructure and Potential Application in CO2 Separation. *J. Membr. Sci.* **2020**, *602*, 117967.
(24) Pramanik, N. B.; Regen, S. L. Hyperthin Membranes for Gas Separations via Layer-by-Layer Assembly. *Chem. Rec.* **2020**, *20* (3), 163−173.
(25) Risangud, N.; Congdon, T. R.; Keddie, D. J.; Wilson, P.; Kempe, K.; Haddleton, D. M. Polyurea Microcapsules from Isocyanatoethyl Methacrylate Copolymers. *J. Polym. Sci., Part A: Polym. Chem.* **2016**, *54* (17), 2698−2705.
(26) Zhang, C.; Cao, B.; Coleman, M. R.; Li, P. Gas Transport Properties in (6FDA-RTIL)-(6FDA-MDA) Block Copolyimides. *J. Appl. Polym. Sci.* **2016**, *133* (9), 43077.
(27) Kammakakam, I.; Nam, S.; Kim, T.-H. PEG−Imidazolium-Functionalized 6FDA−Durene Polyimide as a Novel Polymeric Membrane for Enhanced CO 2 Separation. *RSC Adv.* **2016**, *6* (37), 31083−31091.
(28) Chen, J.-C.; Wu, J.-A.; Chen, K.-H. Synthesis and Characterization of Novel Imidazolium-Functionalized Polyimides for High Temperature Proton Exchange Membrane Fuel Cells. *RSC Adv.* **2016**, *6* (40), 33959−33970.
(29) Mittenthal, M. S.; Flowers, B. S.; Bara, J. E.; Whitley, J. W.; Spear, S. K.; Roveda, J. D.; Wallace, D. A.; Shannon, M. S.; Holler, R.; Martens, R.; Daly, D. T. Ionic Polyimides: Hybrid Polymer Architectures and Composites with Ionic Liquids for Advanced Gas Separation Membranes. *Ind. Eng. Chem. Res.* **2017**, *56* (17), 5055−5069.
(30) Abbott, L. J.; Hart, K. E.; Colina, C. M. Polymatic: A Generalized Simulated Polymerization Algorithm for Amorphous Polymers. *Theor. Chem. Acc.* **2013**, *132* (3), 1334.
(31) Shripad, B.; Wang, B.; Luedtke, G.; Spyvee, M. Heparan Sulfate Biosynthesis Inhibitors for the Treatment Of Diseases. WO 2016057834 A1, 2016.
(32) Polarity Index. https://macro.lsu.edu/howto/solvents/polarity%20index.htm.
(33) Shaplov, A. S.; Lozinskaya, E. I.; Ponkratov, D. O.; Malyshkina, I. A.; Vidal, F.; Aubert, P.-H.; Okatova, O. V.; Pavlov, G. M.; Komarova, L. I.; Wandrey, C.; Vygodskii, Y. S. Bis-(Trifluoromethylsulfonyl)Amide Based "Polymeric Ionic Liquids": Synthesis, Purification and Peculiarities of Structure−Properties Relationships. *Electrochim. Acta* **2011**, *57*, 74−90.
(34) Marcilla, R.; Alberto Blazquez, J.; Rodriguez, J.; Pomposo, J. A.; Mecerreyes, D. Tuning the Solubility of Polymerized Ionic Liquids by Simple Anion-exchange Reactions. *J. Polym. Sci., Part A: Polym. Chem.* **2004**, *42* (1), 208−212.
(35) Arnold, C. Stability of High-temperature Polymers. *J. Polym. Sci. Macromol. Rev.* **1979**, *14* (1), 265−378.
(36) Cella, J. A. Degradation and Stability of Polyimides. *Polym. Degrad. Stab.* **1992**, *36* (2), 99−110.
(37) O'Harra, K. E.; Kammakakam, I.; Bara, J. E.; Jackson, E. M. Understanding the Effects of Backbone Chemistry and Anion Type on the Structure and Thermal Behaviors of Imidazolium Polyimide-ionenes. *Polym. Int.* **2019**, *68* (9), 1547−1556.
(38) Yin, H.; Yang, B.; Chua, Y. Z.; Szymoniak, P.; Carta, M.; Malpass-Evans, R.; McKeown, N. B.; Harrison, W. J.; Budd, P. M.; Schick, C.; Böhning, M.; Schönhals, A. Effect of Backbone Rigidity on the Glass Transition of Polymers of Intrinsic Microporosity Probed by Fast Scanning Calorimetry. *ACS Macro Lett.* **2019**, *8* (8), 1022−1028.
(39) Nofal, M. M.; Aziz, S. B.; Hadi, J. M.; Abdulwahid, R. T.; Dannoun, E. M. A.; Marif, A. S.; Al-Zangana, S.; Zafar, Q.; Brza, M. A.; Kadir, M. F. Z. Synthesis of Porous Proton Ion Conducting Solid Polymer Blend Electrolytes Based on PVA: CS Polymers: Structural, Morphological and Electrochemical Properties. *Materials* **2020**, *13* (21), 4890.
(40) Başdemir, S.; Gültekin, O.; Dal, H. Coupled Thermo-viscoplastic Fracture Model for Ductile-brittle Failure of Amorphous Glassy Polymers with Phase-field Approach. *PAMM* **2023**, *22* (1), No. e202200280.
(41) Hasegawa, M.; Fujii, M.; Ishii, J.; Yamaguchi, S.; Takezawa, E.; Kagayama, T.; Ishikawa, A. Colorless Polyimides Derived from 1S,2S,4R,5R-Cyclohexanetetracarboxylic Dianhydride, Self-Orientation Behavior during Solution Casting, and Their Optoelectronic Applications. *Polymer* **2014**, *55*, 4693.
(42) Kim, G.; Byun, S.; Yang, Y.; Kim, S.; Kwon, S.; Jung, Y. Film Shrinkage Inducing Strong Chain Entanglement in Fluorinated Polyimide. *Polymer* **2015**, *68*, 293.
(43) Robeson, L. M. Correlation of Separation Factor versus Permeability for Polymeric Membranes. *J. Membr. Sci.* **1991**, *62* (2), 165−185.
(44) Robeson, L. M. The Upper Bound Revisited. *J. Membr. Sci.* **2008**, *320* (1−2), 390−400.

https://doi.org/10.1021/acs.macromol.4c02315
Macromolecules 2024, 57, 11085−11096